Emergent self-duality in a long-range critical spin chain: From deconfined criticality to first-order transition

Sheng Yang,[1,*] Zhiming Pan,[2,*] Da-Chuan Lu,[3,†] and Xue-Jia Yu[4,5,‡]

[1]*Zhejiang Institute of Modern Physics and School of Physics, Zhejiang University, Hangzhou 310027, China*
[2]*Institute for Theoretical Sciences, WestLake University, Hangzhou 310024, China*
[3]*Department of Physics, University of California, San Diego, California 92093, USA*
[4]*Department of Physics, Fuzhou University, Fuzhou 350116, Fujian, China*
[5]*Fujian Key Laboratory of Quantum Information and Quantum Optics, College of Physics and Information Engineering, Fuzhou University, Fuzhou, Fujian 350108, China*

(Received 8 September 2023; revised 11 November 2023; accepted 7 December 2023; published 21 December 2023)

Over the past few decades, tremendous efforts have been devoted to understanding self-duality at the quantum critical point, which enlarges the global symmetry and constrains the dynamics. A one-dimensional spin chain is an ideal platform for the theoretical investigation of these exotic phenomena, due to powerful simulation methods such as the density matrix renormalization group. Deconfined quantum criticality with self-duality at the critical point has been found in an extended short-range spin chain. In this work, we employ large-scale density matrix renormalization group simulations to investigate a critical spin chain with long-range power-law interaction $V(r) \sim 1/r^{\alpha}$. Remarkably, we reveal that the long-range interaction drives the original deconfined criticality towards a first-order phase transition as α decreases. More strikingly, the emergent self-duality leads to an enlarged symmetry and manifests at these first-order critical points. This discovery is reminiscent of self-duality protected multicritical points, and it provides an example of the critical line with generalized symmetry. Our work has far-reaching implications for ongoing experimental efforts in Rydberg atom quantum simulators.

DOI: 10.1103/PhysRevB.108.245152

I. INTRODUCTION

Quantum critical points (QCPs) and associated emergent phenomena in strongly correlated many-body systems stand as central topics within realms of both condensed matter and high-energy communities [1–3]. A special property observed in certain QCPs is self-duality. Its origin can trace back to the Kramers-Wannier duality of the two-dimensional (2D) classical Ising model [4,5], and it has subsequently been established in a series of models featuring deconfined quantum critical points (DQCPs) [6–17]. More specifically, DQCPs exhibit anomalies [18], fractionalization [19], self-duality [12,20], and emergent symmetry [21–23]. Despite extensive theoretical [12,16,24–39], numerical [40–75], and experimental explorations [76–78], there are still ongoing efforts surrounding how exactly they have been implemented in lattice models and experimental setups.

Recently, quantum simulators such as Rydberg atoms and ion traps have emerged as powerful tools for simulating exotic quantum phases and phase transitions [79–89]. These systems offer intriguing opportunities for exploring long-range interactions in many-body systems, an area extensively investigated in condensed matter and ultracold atom physics [90–97]. The critical behavior of long-range interacting systems has been widely studied in both quantum spin models [98–112] and interacting fermion models [113–116]. The presence of long-range interactions can effectively modify the system's dimensionality [91,94,99,100,107], leading to effects such as the breakdown of quantum-classical correspondence and the Mermin-Wagner theorem [105,106,109,110], thus they can dramatically alter the phases and phase transitions. For instance, even in the case of conventional QCPs, the influence of long-range interactions generally gives rise to three distinct universality classes [91]: the mean-field universality class, the long-range "nonclassical" universality class, and the short-range universality class. Certainly, a crucial question arises: How do long-range interactions influence unconventional QCPs such as the DQCP? Does this interaction lead to new physical phenomena? Currently, these questions remain unanswered.

In this work, we address the fate of a 1D DQCP with long-range power-law decay interaction $V(r) \sim \frac{1}{r^{\alpha}}$, using both lattice simulations of a frustrated quantum spin model and renormalization-group (RG) calculations of a proposed Luttinger-liquid field theory. Remarkably, we find that there still exist DQCPs and emergent symmetry for fast decay of the long-range interaction above a critical power $\alpha_c \approx 1.95$. This result is consistent with the predictions from bosonization and RG analyses. The most intriguing observation is that as the long-range interaction decays slower (i.e., $\alpha < \alpha_c$), the DQCP turns into a first-order phase transition with enlarged symmetry preserved by the emergent self-duality. This discovery

*These authors contributed equally to this work.
†dclu137@gmail.com
‡xuejiayu@fzu.edu.cn

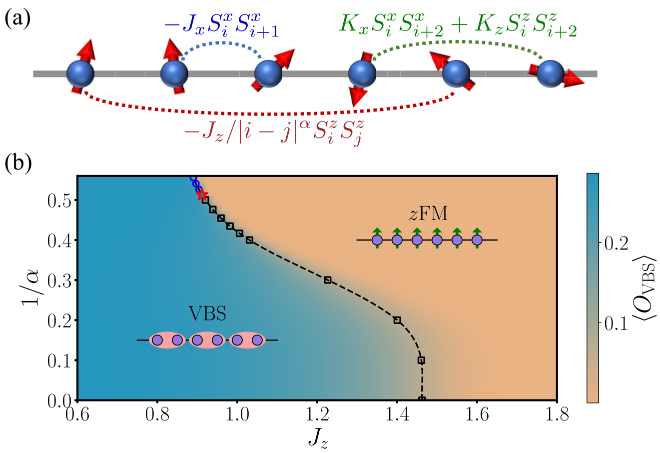

FIG. 1. (a) Schematic representation of the long-range JM model. (b) Phase diagram of the 1D spin Hamiltonian (1), mapped out by the VBS order parameter with $L = 128$. The markers obtained from the extrapolation of $U_{z\mathrm{FM}}$ crossing points demarcate the boundaries between the zFM and VBS ordered phases, and the dashed line is a guide to the eye (see Figs. 6 and 8 for the details). The black squares indicate the continuous phase transition, while the blue circles indicate the first-order phase transition ($\alpha < \alpha_c$ with the estimated multicritical point $\alpha_c \approx 1.95$ marked by the red star).

goes beyond traditional understandings, particularly as emergent symmetry is generally associated with continuous QCPs. Our work clarifies and significantly extends the discussion of the DQCP phenomena in long-range interacting systems, and its signatures should be detectable in existing Rydberg atom experiments.

The rest of this paper is organized as follows: Sec. II presents the lattice model of the 1D DQCP with long-range power-law interaction, and it outlines the employed numerical method. Sections III and IV depict the phase diagram of the 1D DQCP with long-range interaction and the finite-size scaling of the critical behavior, along with an effective field theory to explain the aforementioned numerical results. The discussion and conclusion are presented in Sec. V. Additional data for our analytical and numerical calculations are provided in the Appendixes.

II. MODEL AND METHOD

The system under study is a frustrated quantum spin chain proposed by Jiang and Motrunich (the JM model) [15], with additional long-range power-law interactions, depicted in Fig. 1(a). The model is defined by the following Hamiltonian:

$$H_{\mathrm{LRJM}} = \sum_i \left(-J_x S_i^x S_{i+1}^x + K_x S_i^x S_{i+2}^x + K_z S_i^z S_{i+2}^z\right) - \frac{J_z}{N(\alpha)} \sum_{i<j} \frac{S_i^z S_j^z}{|i-j|^\alpha}, \tag{1}$$

where $\boldsymbol{S}_i = (S_i^x, S_i^y, S_i^z)$ represents the spin-1/2 operator on each site i. J_γ/K_γ ($\gamma = x, z$) corresponds to the nearest/next-nearest-neighbor ferromagnetic (FM)/antiferromagnetic (AFM) couplings. For simplicity, we set $K_x = K_z = 0.5$ and $J_x = 1.0$ as the energy unit below. The parameter α tunes the power of long-range $S^z - S^z$ interactions, which tends to the nearest-neighbor short-range JM model in the limit $\alpha \to \infty$. The Kac factor $N(\alpha)(= \frac{1}{L-1}\sum_{i<j}\frac{1}{|i-j|^\alpha})$ is included to keep the Hamiltonian extensive.

When $\alpha \to \infty$, the original JM model exhibits a 1+1D analogy of DQCP [15,69,117,118]. By tuning J_z, the system undergoes a continuous quantum phase transition between a valence-bond-solid (VBS) phase ($J_z \approx 1$) and a spin-ordered ferromagnetic (called zFM) phase ($J_z \gg 1$), which corresponds to the horizontal line $1/\alpha = 0$ in Fig. 1(b). The phase transition is analogous to the 2+1D DQCP [8] as it represents a direct continuous transition between two incompatible spontaneous symmetry breaking phases [15,69]. Moreover, it can be analytically described by a Luttinger-like field theory with central charge $c = 1$, featuring an emergent $\mathrm{O}(2) \times \mathrm{O}(2)$ symmetry at the deconfined critical point [118].

To obtain the ground-state properties of the Hamiltonian H_{LRJM}, we adopt the density matrix renormalization group (DMRG) [119–121] based on the matrix product state (MPSs) technique [121,122], which has established itself as one of the best numerical approaches nowadays for one-dimensional strongly correlated systems. Our focus lies in exploring the resulting critical behaviors arising from the interplay between the DQCP and long-range interactions. For most of the calculations, we consider system sizes $L = 32$–256, while for reliable finite-size scaling analyses, we simulate systems of size $L = 192$–384. To guarantee the numerical accuracy and efficiency in practical calculations, we perform at most 50 DMRG sweeps with a gradually increased MPS bond dimension, $\chi \leqslant \chi_{\max} = 2048$, under the open boundary condition. Once the MPS energy has converged up to the order 10^{-10}, the sweeping route would be stopped and the final MPS is believed to be a faithful representation of the true ground state.

III. NUMERICAL RESULTS

A. Quantum phase diagram: An overview

Before the illustration of the numerical results, we first summarize the main findings about the long-range JM model in Eq. (1). An accurate ground-state phase diagram expanded by the axes of $1/\alpha$ and J_z is displayed in Fig. 1(b). It is found that the long-range interaction physics can be classified into two distinct regimes separated by a critical power α_c. For $\alpha > \alpha_c$, the long-range power-law interaction decays very fast such that the interaction tail does not bring any essential change to the DQCP compared with the original model with nearest interaction. The VBS-to-zFM transition remains a direct continuous transition characterized by DQCP properties. This large-α regime is in some sense roughly consistent with the classification given in Ref. [91], which asserts that if α is larger than a certain critical value, the critical behavior should be indistinguishable from its short-range limit. However, the long-range interaction does extend the zFM phase region, and the critical point shifts gradually towards smaller J_z with decreasing α, as expected. Remarkably, what makes our results fundamentally different from the previous literature (see Ref. [91] and references therein) is the small-α regime. For the case of $\alpha < \alpha_c$, the phase transition is no longer continuous but is now driven into a first-order one by the sufficiently

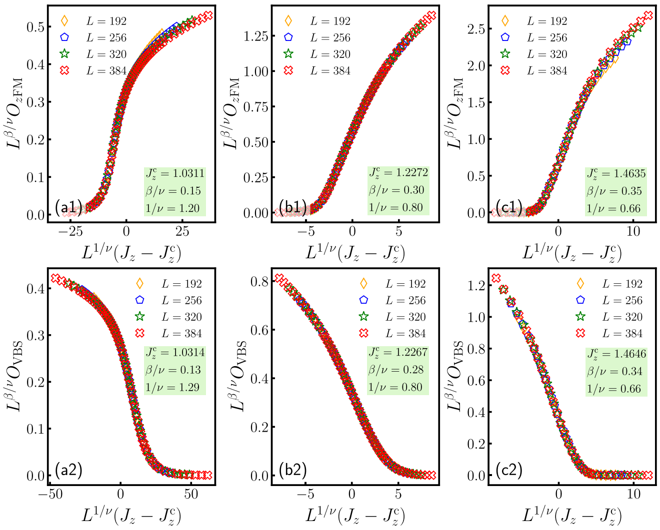

FIG. 2. The finite-size scaling analysis of order parameters $O_{z\mathrm{FM}}$ and O_{VBS} for the long-range JM model with $\alpha = 2.50$ [(a1),(a2)], $\alpha = 3.33$ [(b1),(b2)], and $\alpha = +\infty$ [(c1),(c2)].

strong long-range interaction. More strikingly, our numerical calculations and low-energy field theory analysis consistently support that the self-duality that emerged at the 1+1D DQCP survives from the strong long-range interaction, giving rise to a first-order phase transition with an enlarged $\mathrm{O}(2) \times \mathrm{O}(2)$ symmetry, which is not well-studied in previous works.

B. Continuous phase transition at $\alpha > \alpha_c$

Similar to the case of conventional QCPs, it is found that the 1+1D analogy of the DQCP hosted in the original short-range JM model is robust against the long-range interaction when the power α is large enough.

To unveil the continuous nature of the transition, we calculate the associated order parameters, respectively, given by

$$O_{z\mathrm{FM}} = \frac{1}{L'} \sum_i S_i^z \quad \text{and} \quad O_{\mathrm{VBS}} = \frac{1}{L'} \sum_i (-1)^i \boldsymbol{S}_i \cdot \boldsymbol{S}_{i+1}, \tag{2}$$

where the summation is restricted within the middle $L' = L/2$ subsystem to reduce the boundary effect, and we resort to standard finite-size scaling analyses according to the scaling form [123]

$$\langle O_{z\mathrm{FM/VBS}} \rangle = L^{-\beta/\nu} f\big[L^{1/\nu}\big(J_z - J_z^c\big)\big], \tag{3}$$

where β and ν are critical exponents of order parameter and correlation length, respectively. If the phase transition is continuous, the critical exponents extracted independently from the data collapses of $O_{z\mathrm{FM}}$ and O_{VBS} should be identical.

As elaborated in Fig. 2, we have performed conventional finite-size scaling analysis for several representative α values. It is noted that we have added a pinning field of strength 1 at both boundaries when we calculate the zFM order parameter, and we also further restrict the summation in Eq. (2) within the central two sites to minimize the boundary effect as much as we can. Similar to Refs. [124,125], we first adjust the exponent $\eta = \beta/\nu$ such that the curves $L^{\eta}\langle O_x \rangle$ as a function of J_z intersect with each other for all system sizes, and J_z^c can be estimated by the crossing point. Then we adjust the exponent $1/\nu$ until a good collapse of $L^{\eta}\langle O_x \rangle$ versus $L^{1/\nu}(J_z - J_z^c)$ for all L is achieved.

Following the detailed procedure, we present final data collapses of the order parameters in Fig. 2. It is evident that both order parameters obey the standard scaling relation (3) quite well, and the extracted critical exponents β/ν are in agreement with each other within numerical accuracy, corroborating that the 1+1D DQCP hosted in the original JM model is robust against the long-range S^z-S^z interaction when $\alpha > \alpha_c$. It is also interesting to notice that the exponents $\eta \equiv \beta/\nu$ and ν both decrease gradually with increasing $1/\alpha$, but the equality $2\nu(1 - 2\eta) = 1$ still holds roughly for all the α values examined here, which is consistent with the prediction from the dual Luttinger-like theory calculations shown below.

C. First-order phase transition at $\alpha < \alpha_c$

Different from the large-α regime, the VBS-to-zFM phase transition evolves from continuous to first order as the power α is decreased smaller than a certain critical value α_c, which is beyond the conventional classification of the critical behaviors affected by long-range interactions (see Sec. I or Ref. [91]).

A faithful quantity commonly used to distinguish between the continuous and first-order phase transitions is the Binder ratio U [126], which is defined by (for the zFM order here)

$$U_{z\mathrm{FM}} = \frac{1}{2}\left(3 - \frac{\langle O_{z\mathrm{FM}}^4 \rangle}{\langle O_{z\mathrm{FM}}^2 \rangle^2}\right). \tag{4}$$

This observable has a vanishing scaling dimension and hence it can give reliable information on the nature and position of the QCP. For continuous phase transitions, $U_{z\mathrm{FM}}$ typically shows a monotonic behavior, while for first-order phase transitions, $U_{z\mathrm{FM}}$ displays instead a nonmonotonic behavior and exhibits a diverged negative peak near the QCP with increasing system size [127–129].

As shown in Figs. 3(a) and 3(b) and Fig. 6, it is found that there exists a critical value $\alpha_c \approx 1.95$, such that when $\alpha > \alpha_c$, the Binder ratio $U_{z\mathrm{FM}}$ shows a monotonic growth as J_z is increased, but when $\alpha < \alpha_c$, $U_{z\mathrm{FM}}$ exhibits a nonmonotonic behavior with J_z and develops a diverged negative peak near the transition point. The distinct behaviors of $U_{z\mathrm{FM}}$ imply that the quantum phase transition changes into a first-order type as α is decreased smaller than α_c. Furthermore, the precise critical point J_z^c can be determined by extrapolation based on the relation $J_z^*(L) = J_z^c + aL^{-b}$, where $J_z^*(L)$ is the crossing point of $U_{z\mathrm{FM}}(L)$ and $U_{z\mathrm{FM}}(L + 32)$ [128]. In Figs. 3(c) and 3(d), one can see a similar diverged negative peak developed in the VBS Binder ratio, $U_{\mathrm{VBS}} = (3 - \langle O_{\mathrm{VBS}}^4 \rangle / \langle O_{\mathrm{VBS}}^2 \rangle^2)/2$, and the critical points obtained independently from $U_{z\mathrm{FM}}$ and U_{VBS} are close to each other. Other results of such least-squares fitting are included in Appendix C, and the estimated critical points are used to demarcate the phase boundaries in Fig. 1(b).

To further confirm the first-order phase transition that occurred at $\alpha < \alpha_c$, in Fig. 3(e) we also calculate the ground-state energy density e_g and its corresponding first derivative $\partial e_g / \partial J_z$ near the transition point for $\alpha = 1.8$. It is found that the first-derivative curves are more and more steep, and a distinct jump is expected in the thermodynamic limit, which

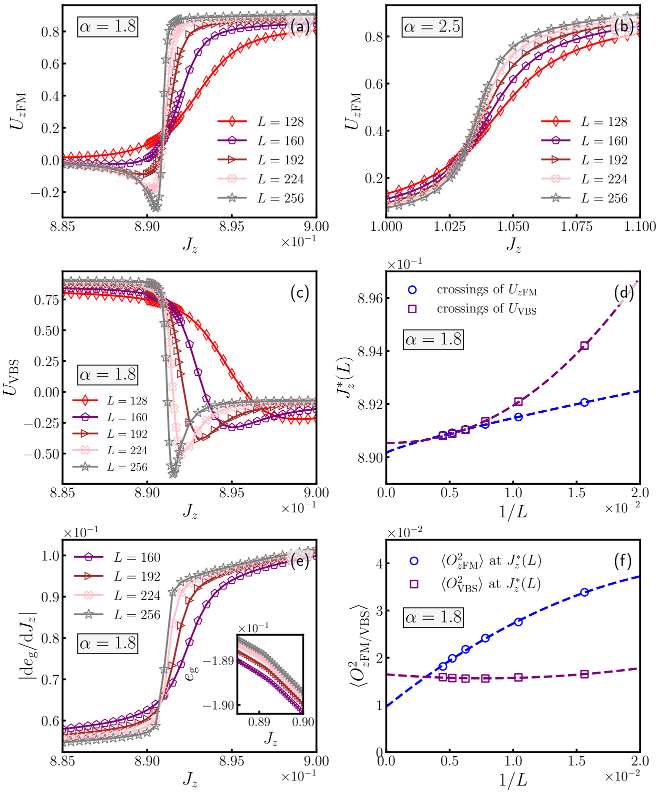

FIG. 3. (a),(b) The Binder ratio of the magnetization $U_{z\mathrm{FM}}$ vs J_z. (c) The Binder ratio of the VBS order U_{VBS} vs J_z. (d) The crossing points $J_z^*(L)$ of $U_x(L)$ and $U_x(L+32)$ ($x = z$FM or VBS) are displayed vs $1/L$. The dashed curves are least-squares fit according to $J_z^*(L) = J_z^c + aL^{-b}$. (e) The ground-state energy per site and its first derivative with respect to J_z. (f) The squared order parameter $\langle O_x^2\rangle$ ($x = z$FM or VBS) at the finite-size pseudocritical points $J_z^*(L)$. The curves are second-order polynomial fits. Parts (a) and (c)–(f) are plotted for $\alpha = 1.8$, but (b) is plotted for $\alpha = 2.5$.

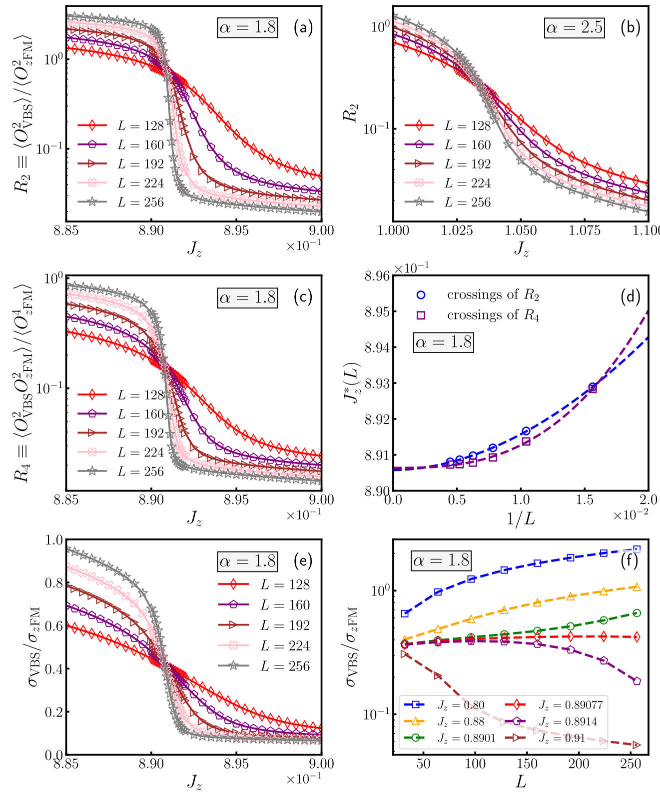

FIG. 4. (a),(b) The ratio of the squared order parameters R_2 vs J_z. (c) The cross ratio of the squared order parameters R_4 vs J_z. (d) The crossing locations $J_z^*(L)$ of $R_{2/4}(L)$ and $R_{2/4}(L+32)$ are shown vs $1/L$. The dashed curves are least-squares fit according to the relation $J_z^*(L) = J_z^c + aL^{-b}$. (e) The variance ratio $\sigma_{\mathrm{VBS}}/\sigma_{z\mathrm{FM}}$, where $\sigma_x \equiv (\langle O_x^4\rangle - \langle O_x^2\rangle^2)^{1/2}$ ($x = z$FM or VBS), as a function of J_z for several system sizes. (f) The ratio $\sigma_{\mathrm{VBS}}/\sigma_{z\mathrm{FM}}$ as a function of L for several J_z near the critical point J_z^c. Parts (a) and (c)–(f) are plotted for $\alpha = 1.8$, but (b) is plotted for $\alpha = 2.5$.

is definite evidence of first-order phase transitions. Moreover, order parameters at their respective pseudocritical points $J_z^*(L)$ (i.e., crossing points of $U_{z\mathrm{FM}}$ and U_{VBS}) are displayed versus $1/L$ in Fig. 3(f). The coexistence of zFM and VBS orders at the critical point can be another decisive indicator of the first-order transition.

In summary, all the elaborated results consistently corroborate a first-order phase transition in the small-α regime. As we have examined the observed phase transition from three different perspectives, each of which has been used as the main evidence for first-order transitions in many works, the first-order transition found here should be reliable with these self-consistent results. It is also worth mentioning that a bimodal histogram of energy or certain quantities may give other evidence for the first-order transition, however, such an illustration seems not to be practicable within the adopted DMRG framework fundamentally distinct from the sampling-based Monte Carlo simulation. On the other hand, in the present work, we only focus on the properties of the first-order and continuous transitions. The tricritical point α_c is very interesting and can be studied by the flowgram method developed in [130], but we leave it for future investigations.

D. Enlarged symmetry on the critical line

One of the most significant features of the 1+1D DQCP in the original short-range JM model is the $\mathrm{O}(2) \times \mathrm{O}(2)$ symmetry that emerged exactly at the deconfined critical point [15,69,118]. Therefore, it is natural to ask whether this enlarged symmetry still exists at the QCPs of the long-range JM model.

For this purpose, we calculate the ratio of the squared order parameters defined by $R_2 = \langle O^2_{\mathrm{VBS}}\rangle/\langle O^2_{z\mathrm{FM}}\rangle$. According to Refs. [22,59,131,132], if the VBS and zFM order parameters have the same scaling dimension, the ratio R_2 should be size-independent at the transition point, and the QCP would have an enlarged symmetry that rotates these two orders. The results of R_2 are detailed and summarized in Figs. 4(a) and 4(b) and Fig. 7; it is obvious that R_2 becomes size-independent near the QCP for all α, indicating that the VBS-to-zFM transition still hosts the $\mathrm{O}(2) \times \mathrm{O}(2)$ symmetry even when its nature has been driven into first-order. Similarly, as shown in Figs. 4(c) and 4(d), the cross ratio of order parameters, $R_4 = \langle O^2_{\mathrm{VBS}}O^2_{z\mathrm{FM}}\rangle/\langle O^4_{z\mathrm{FM}}\rangle$, of different system sizes also intersects with each other roughly at a single point, and the extrapolation of the pseudocritical point is also close to the one obtained from the ratio R_2.

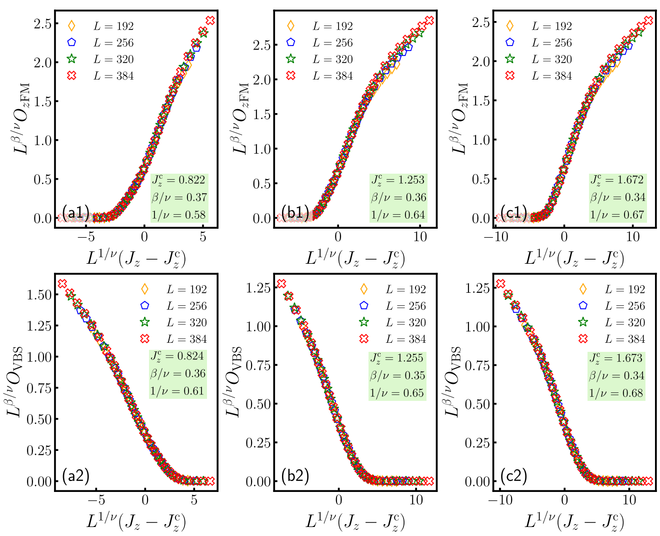

FIG. 5. The finite-size scaling analysis of order parameters $O_{z\rm FM}$ and $O_{\rm VBS}$ for the original JM model with $K_z = 0.2$ [(a1),(a2)], $K_z = 0.4$ [(b1),(b2)], and $K_z = 0.6$ [(c1),(c2)].

In Fig. 4(e), we also examine the variance ratio $\sigma_{\rm VBS}/\sigma_{z\rm FM}$, where $\sigma_x = (\langle O_x^4\rangle - \langle O_x^2\rangle^2)^{1/2}$ [22,133], which is another useful detector for symmetries at QCPs. Similar to R_2, we can indeed see an intersection of $\sigma_{\rm VBS}/\sigma_{z\rm FM}$ curves of all L at the transition point. Figure 4(f) explicitly shows the dependence of $\sigma_{\rm VBS}/\sigma_{z\rm FM}$ on L near the critical point. The universal behavior of $\sigma_{\rm VBS}/\sigma_{z\rm FM}$ around $J_z \approx 0.8908$ gives additional evidence for the enlarged $\mathrm{O}(2)\times\mathrm{O}(2)$ symmetry at the first-order phase transition.

Until now, the presented numerical simulations have been consistent with each other and pointed to a first-order phase transition with enlarged $\mathrm{O}(2)\times\mathrm{O}(2)$ symmetry beyond conventional understandings. Therefore, it is necessary to explain our results, and the key point is the emergent self-duality that survived from the long-range interaction, which preserves the $\mathrm{O}(2)\times\mathrm{O}(2)$ symmetry.

E. Transition nature of the original JM model with $K_z \neq 1/2$

Before the presentation of the low-energy field theory analysis, it is also necessary to verify that the observed first-order phase transition is not induced by the naive modification of K_z, since the inclusion of the long-range S^z-S^z interaction in the JM model can effectively change the value of K_z. For this purpose, we investigate the quantum phase transition of the *original* JM model with the parameter setting, $J_x = 1$, $K_x = 1/2$, and $K_z \neq 1/2$.

Following the same procedure explained in Sec. III B, we utilize the standard finite-size scaling analysis according to Eq. (3) to extract the quantum critical point J_z^c and related critical exponents, β and ν. As summarized in Fig. 5, it is clear that the obtained critical exponents β/ν are almost identical for zFM and VBS orders, which is a key property of the DQCP theory [15], indicating that the quantum phase transition is still continuous. As the effective value of K_z modified by the long-range S^z-S^z interaction, $K_z^{\rm eff} = 1/2 - J_z/[2^\alpha N(\alpha)]$, is larger than 0.2 at the critical point for $\alpha = 1.8$, the results shown here can support that the first-order phase transition found in the long-range JM model at $\alpha = 1.8$ is indeed induced by the long-range S^z-S^z interaction, thus ruling out the possibility that the first-order transition is caused by a naive modification of the coupling K_z in the original JM model.

IV. LOW-ENERGY EFFECTIVE THEORY

The phase transition between the zFM and VBS orders is second order when α is large and first order when α is small. The continuous to first-order transition happens at the critical power α_c. This continuous to first-order transition is driven by the long-range S^z-S^z interaction. According to the bosonization method [15,117,134] (see Appendix A for the details), the spin operators can be represented by a bosonic field ϕ in the continuous limit,

$$S_j^z \sim \cos\phi(x)/2, \quad S_j^x \sim -\sin\phi(x)/2, \tag{5}$$

where the discrete coordinate is replaced by its continuous version, $x_j \to x$. Thus, the 1D long-range S^z-S^z interaction takes the following form in the effective continuum theory [109]:

$$\sum_{i,j}\frac{S_i^z S_j^z}{|i-j|^\alpha} \sim \int dxdy\frac{\cos[\phi(x)]\cos[\phi(y)]}{4|x-y|^\alpha}, \tag{6}$$

where x, y are the 1D continuous coordinates. The effective action in the Euclidean path integral formulation under bosonization is given by [15,134]

$$S = \int d\tau\, dx\left[\frac{i}{\pi}\partial_\tau\phi\partial_x\theta + \frac{v}{2\pi}\left(\frac{1}{g}(\partial_x\theta)^2 + g(\partial_x\phi)^2\right)\right] + \int d\tau\, dx\,[\lambda_u\cos(4\theta) + \lambda_a\cos(2\phi)] + S_{\rm LR}, \tag{7}$$

with imaginary time τ, spatial coordinates x, velocity v, and Luttinger parameter g. λ_u and λ_a are the most relevant short-range interactions, which preserve the symmetry of the JM model. The long-range part in the Lagrangian is deduced from Eq. (6),

$$S_{\rm LR} = \frac{\lambda_+}{2}\int d\tau dx dr\frac{1}{|r|^\alpha}\cos[\phi(x+r,\tau)+\phi(x,\tau)] + \frac{\lambda_-}{2}\int d\tau dx dr\frac{1}{|r|^\alpha}\cos[\phi(x+r,\tau)-\phi(x,\tau)], \tag{8}$$

where r denotes the relative distance of the fields. Here, the cos - cos correlation in Eq. (6) has been separated into two parts, whose effects would be different. For smaller interaction range r, λ_- will contribute to the renormalization of the Luttinger parameters. We would focus on the renormalization of the long-range contribution, and we can omit this shorter-range r contribution at this stage. Moreover, it should also be noticed that the Luttinger parameter g could be a nonuniversal quantity at the critical point. While for the pure XXZ model, the explicit value of g could be deduced from the microscopic parameters based on the Bethe ansatz [135–137], for the general spin model, e.g., for the JM model with long-range interaction, it would be hard to determine the explicit value of g from the microscopic parameters.

Based on the RG analysis (in Appendix B), the long-range S^z-S^z interaction Eq. (8) is irrelevant or less relevant than the short-range one when the exponent is greater than some critical value, $\alpha > \alpha_c$. In the large-α regime, the continuous transition between the VBS and zFM phases driven by short-range interaction [15] is stable against the long-range perturbation. On the other hand, when α is smaller than the critical value, the long-range S^z-S^z interaction becomes the most relevant operator of the system, and it drives the continuous transition to a first-order transition. To decode the nontrivial transition between the VBS and zFM phases, it will be more sufficient to work in the effective dual theory formulation, as was done in the original JM model [15,69,117,118].

A. Dual field theory

The dual field theory description plays an important role for understanding the 1D DQCP nature of the JM model [15]. Especially, the continuous transition between VBS and zFM phases in the original JM model has emergent self-duality, as shown in [15,69,117,118], since the scaling dimensions of the two order parameters are the same in both numerical and theoretical calculations. While the construction of the dual theory field requires much effort, the final formulation is direct and simple, that is, the z-FM and VBS order parameters could be represented by the continuous dual field $\tilde{\theta}$ as $\Psi_{z\text{FM}} \sim \sin(\tilde{\theta})$ and $\Psi_{\text{VBS}} \sim \cos(\tilde{\theta})$ [15]. The dual field theory unifies zFM and VBS order parameters together by the single field $\tilde{\theta}$. The self-duality manifests in the dual Luttinger liquid theory in the imaginary-time path integral action [15,134],

$$\tilde{S} = \int d\tau\, dx \left[\frac{i}{\pi}\partial_\tau\tilde{\phi}\partial_x\tilde{\theta} + \frac{\tilde{v}}{2\pi}\left(\frac{1}{\tilde{g}}(\partial_x\tilde{\theta})^2 + \tilde{g}(\partial_x\tilde{\phi})^2\right)\right] + \int d\tau\, dx\,[\tilde{\lambda}\cos(2\tilde{\theta})] + \tilde{S}_{LR}, \tag{9}$$

with the $(1+1)$D spatial-time coordinates (x,τ), effective velocity $\tilde{v}$, and Luttinger parameter $\tilde{g}$. The tilde symbol is used to emphasize the difference from the original field theory in Eq. (9). $(\tilde{\theta},\tilde{\phi})$ is a pair of conjugate fields in the dual field theory [15]. We first summarized some basic results in the short-range system without $\tilde{S}_{\text{LR}}$ [15,69,117,118]. Since the relevant problem lying in the parameter regime $\tilde{g} \in (1/2, 2)$, $\tilde{\lambda}$ is the only relevant short-ranged operator that could drive the phase transition between the z-FM and VBS orders. A relevant positive (negative) $\tilde{\lambda}$ will pin down the dual field $\tilde{\theta} = \frac{\pi}{2}$ ($\tilde{\theta} = 0$), which corresponds to the zFM (VBS) phase, $\Psi_{z\text{FM}} \neq 0$ ($\Psi_{\text{VBS}} \neq 0$). On the contrary, $\tilde{\phi}$ field could be fully integrated out in the path integral since its interaction term is irrelevant in the critical theory, leading to a pure sine-Gordon theory for the field $\tilde{\theta}$. Instantly, zFM and VBS order parameters have the same scaling dimensions $\dim[\Psi_{z\text{FM}}] = \dim[\Psi_{\text{VBS}}] = \tilde{g}/4$ [15,69]. The emergent self-duality permutes VBS and zFM order parameters. Combined with the global symmetry O(2), the emergent self-duality promotes the global symmetry to $\mathrm{O}(2) \times \mathrm{O}(2)$.

From the above numerical simulations, the substantial evidence shows that the emergent self-duality still persists in the first-order transition when the long-range S^z-S^z interaction is relevant. Indeed, the long-range S^z-S^z interaction is effectively self-dual preserving at the critical point. Based on the dual bosonization approach, the long-range S^z-S^z interaction in the dual theory is represented as

$$\tilde{S}_{\text{LR}} = \frac{\tilde{\lambda}_-}{2}\int d\tau dx dr \frac{1}{|r|^\alpha}\cos[\tilde{\theta}(x+r,\tau) - \tilde{\theta}(x,\tau)] - \frac{\tilde{\lambda}_+}{2}\int d\tau dx dr \frac{1}{|r|^\alpha}\cos[\tilde{\theta}(x+r,\tau) + \tilde{\theta}(x,\tau)]. \tag{10}$$

Here, the effective coupling $\tilde{\lambda}_-$ drives the system to a spatial uniform pattern, while the sign of $\tilde{\lambda}_+$ leads to the VBS or zFM order. In the infrared limit, long-range $\tilde{\lambda}_+$ has a similar effect to the short-range $\tilde{\lambda}$, and a combination of them leads to a renormalized driving coupling, which will tune the phase transition between VBS and zFM order. This effective tuning coupling also accounts for the shift of the phase boundary to the left in Fig. 1(b). Under the RG flow (in Appendix B), $\tilde{\lambda}_-$ becomes more relevant than $\tilde{\lambda}_+$, while the VBS-zFM phase transition is still tuned by $\tilde{\lambda}_+$. When the power of long-range interaction becomes smaller than the critical value $\alpha < \alpha_c$, $\tilde{\lambda}_-$ becomes the most relevant operator of the system, driving the second-order transition into a first-order one. Therefore, only $\tilde{\lambda}_-$ affects the infrared fate along the critical line.

Under the self-duality $\sin(\tilde{\theta}) \leftrightarrow \cos(\tilde{\theta})$, the long-range interaction transforms as $\tilde{\lambda}_- \to \tilde{\lambda}_-$, $\tilde{\lambda}_+ \to -\tilde{\lambda}_+$. The $\tilde{\lambda}_-$ term is manifestly self-dual invariant. On the contrary, the $\tilde{\lambda}_+$ term breaks the self-duality and transforms the same as $\tilde{\lambda}$. Along the critical line, the VBS to zFM tuning coupling tends to zero and the system is self-dual invariant in the low-energy field theory. The emergent self-duality persists along the transition line from continuous to first-order transition. This can be understood as the self-duality protected criticality [138]. Since the self-duality permutes the two phases VBS and zFM, the self-duality invariant region should be the interface between them, and that is the phase boundary in Fig. 1(b).

V. DISCUSSIONS AND CONCLUSIONS

We noticed that some researchers have discovered emergent symmetry at special [139,140] or weakly first-order transitions [131,132,141]. They explained that the absence of a free energy barrier allows different orders to transform into each other. However, we emphasize that our model exhibits an unambiguous enlarged $\mathrm{O}(2) \times \mathrm{O}(2)$ symmetry at the strong first-order phase transition, which is different from the previous cases. Our findings reveal that, in the low-energy effective field theory, the self-dual invariant long-range operator changes from being irrelevant to relevant as α decreases, resulting in a first-order critical point with emergent self-duality, which leads to enlarged $\mathrm{O}(2) \times \mathrm{O}(2)$ global symmetry. Additionally, emergent supersymmetry [142] has also been discovered at first-order critical points.

Regarding experimental realization, Lee *et al.* [143] recently proposed a Landau-forbidden quantum phase transition with an emergent symmetry in a one-dimensional strongly interacting array of trapped neutral Rydberg atoms. This can be experimentally observed with measurement snapshots on a standard computational basis.

In conclusion, we perform large-scale DMRG simulations to decipher the critical properties of the JM model with long-range interactions. Our numerical simulation unambiguously demonstrates that the emergent self-duality appears along the critical line, from the continuous transition to the first-order transition. And the self-duality enlarges the global symmetry to $O(2) \times O(2)$. This finding aligns with the Luttinger-liquid theory calculations, where part of the long-range spin-spin interaction becomes the self-dual invariant relevant operator and drives the continuous transition to the first-order transition. This is reminiscent of the tricritical Ising model, where the self-dual invariant operator can drive the tricritical point to either the Ising transition or the first-order transition. In particular, the first-order transition is a gapped phase with three ground-state degeneracies due to the anomalous self-duality [144,145].

We leave for future work the determination of a precise value of α_c, comparisons of universal quantities with long-range interactions through renormalization-group analysis, and a comparative study of the quantum critical behavior at the multicritical point. Our work paves the way for understanding the interplay between unconventional quantum critical points and long-range physics in an experimental and theoretically controlled manner.

ACKNOWLEDGMENTS

We thank Yi-Zhuang You, Zi Yang Meng, Ruben Verresen, and Hai-Qing Lin for very helpful discussions. Numerical simulations were carried out with the ITENSOR package [146] on the Kirin No. 2 High Performance Cluster supported by the Institute for Fusion Theory and Simulation (IFTS) at Zhejiang University. Z.P. is supported by National Natural Science Foundation of China (No. 12147104). X.-J. Yu acknowledges support from the start-up Grant No. 511317 of Fuzhou University.

APPENDIX A: EFFECTIVE THEORY FOR THE 1D SPIN CHAIN WITH SHORT-RANGE INTERACTION

In this Appendix, we summarize the basic effective continuum theory description of the generalized 1D spin-1/2 chain JM model [15,69,117,118],

$$H = \frac{1}{4}\sum_j \left(-J_x\sigma_j^x\sigma_{j+1}^x - J_z\sigma_j^z\sigma_{j+1}^z\right) + \frac{1}{4}\sum_j \left(+K_x\sigma_j^x\sigma_{j+2}^x + K_z\sigma_j^z\sigma_{j+2}^z\right), \tag{A1}$$

where the spin operators have been represented by Pauli matrices $\boldsymbol{S}_j = \frac{1}{2}\boldsymbol{\sigma}_j = \frac{1}{2}(\sigma_j^x, \sigma_j^y, \sigma_j^z)$. The effective field theory could be obtained from the bosonization approach based on the transformation [15,117,134]

$$\sigma_j^y \sim \frac{2}{\pi}(\theta_{j+1/2} - \theta_{j-1/2}), \quad \sigma_j^z \sim \cos(\phi_j), \quad \sigma_j^x \sim -\sin(\phi_j), \quad [\theta_{j+1/2}, \phi_{j'}] = i\pi\Theta(j + 1/2 - j'), \tag{A2}$$

where θ and ϕ are a pair of conjugate fields, and $\Theta(x)$ is a Heaviside step function. Taking the continuum limit, the effective action in the imaginary-time path integral formulation is given by [15]

$$S[\phi,\theta] = \int d\tau\, dx \left[\frac{i}{\pi}\partial_\tau\phi\partial_x\theta + \frac{v}{2\pi}\left(\frac{1}{g}(\partial_x\theta)^2 + g(\partial_x\phi)^2\right)\right] + \int d\tau\, dx\, [\lambda_u\cos(4\theta) + \lambda_a\cos(2\phi)], \tag{A3}$$

where τ is the imaginary time, x is the spatial coordinate, v is the velocity, and g is the Luttinger parameter. λ_u and λ_a are the most relevant operators that have the largest scaling dimension and reflect the symmetries of the system. They will drive the possible transition to the ordered phase, reflecting by the pinning of the (θ, ϕ) fields. In the continuum theory, the order parameters for the z-FM phase and the VBS phase are represented by the continuous bosonic fields

$$\Psi_{z\text{FM}} \sim \cos(\phi), \quad \Psi_{\text{VBS}} \sim \cos(2\theta).$$

The z-FM state $\Psi_{z\text{FM}}$ is invariant under the lattice translational symmetry $T_x(\phi,\theta) \to (\phi, \theta + \pi/2)$ and $\mathbb{Z}_2^z$ spin rotation symmetry around z-axis $g_z(\phi,\theta) \to (-\phi, -\theta)$, but it breaks the $\mathbb{Z}_2^x$ spin rotation symmetry around the x-axis $g_x(\phi,\theta) \to (-\phi + \pi, -\theta)$ and time-reversal symmetry $\mathcal{T}(\phi,\theta,i) \to (\phi + \pi, -\theta, -i)$. The VBS state Ψ_{VBS} is invariant under g_x, g_z, and $\mathcal{T}$, but it breaks T_x. The tree-level scalings of the cos-operators are given by $\dim[\cos(2n\theta)] = n^2 g$ and $\dim[\cos(m\phi)] = \frac{m^2}{4g}$. The tree-level β-functions for the short-ranged λ_u- and λ_a-term are given by

$$\frac{d\lambda_u}{dl} = (2 - \dim[\cos(4\theta)])\lambda_u = (2 - 4g)\lambda_u, \quad \frac{d\lambda_a}{dl} = (2 - \dim[\cos(2\phi)])\lambda_u = \left(2 - \frac{1}{g}\right)\lambda_u. \tag{A4}$$

The scaling behaviors of the zFM correlation and the VBS correlation are given by

$$\langle\Psi_{z\text{FM}}(r)\Psi_{z\text{FM}}(0)\rangle \sim \frac{1}{r^{1/2g}}, \quad \langle\Psi_{\text{VBS}}(r)\Psi_{\text{VBS}}(0)\rangle \sim \frac{1}{r^{2g}}.$$

However, such continuum theory is not complete for the understanding of a deconfined quantum critical point between z-FM and VBS order, and a dual theory is necessary to fully characterize the critical behavior [15].

Dual Luttinger-like theory

To describe the deconfined quantum phase transition between z-FM and VBS order, it is more sufficient to work in the duality formulation, which is also represented by a Luttinger-like theory [15,69],

$$S[\tilde{\phi},\tilde{\theta}] = \int d\tau\, dx \left[\frac{i}{\pi}\partial_\tau\tilde{\phi}\partial_x\tilde{\theta} + \frac{\tilde{v}}{2\pi}\left(\frac{1}{\tilde{g}}(\partial_x\tilde{\theta})^2 + \tilde{g}(\partial_x\tilde{\phi})^2\right)\right] + \int d\tau\, dx\, [\lambda\cos(2\tilde{\theta}) + \lambda'\cos(4\tilde{\theta}) + \kappa\cos(4\tilde{\phi})], \tag{A5}$$

where $\tilde{\phi}$ and $\tilde{\theta}$ are a pair of conjugate fields in the dual theory, and $\tilde{v}$ and $\tilde{g}$ are the corresponding velocity and Luttinger parameter. λ, λ', and κ are several lowest-order short-range interactions.

The phase transition between z-FM and VBS order lies within the regime $\tilde{g} \in (1/2, 2)$ such that the λ-term is the single relevant operator that drives the phase transition when its sign alters. The correlation length exponent at the critical point follows the scaling dimension of $\lambda\cos(2\tilde{\theta})$, that is [15],

$$\nu^{-1} = 2 - \dim[\cos(2\tilde{\theta})] = 2 - \tilde{g}, \quad \nu = \frac{1}{2-\tilde{g}}.$$

In this dual Luttinger-like theory, the order parameters for the z-FM and VBS phase are decoded into a compatible form based on a single field $\tilde{\theta}$,

$$\Psi_{z\mathrm{FM}} \sim \sin(\tilde{\theta}), \quad \Psi_{\mathrm{VBS}} \sim \cos(\tilde{\theta}), \tag{A6}$$

which, of course, have the same scaling dimension $\dim[\Psi_{z\mathrm{FM}}] = \dim[\Psi_{\mathrm{VBS}}] = \tilde{g}/4$ and similar correlation behavior at the critical point,

$$\langle\Psi_{z\mathrm{FM}}(r)\Psi_{z\mathrm{FM}}(0)\rangle \sim \frac{1}{r^{2\dim\Psi_{z\mathrm{FM}}}} = \frac{1}{r^{\tilde{g}/2}}, \quad \langle\Psi_{\mathrm{VBS}}(r)\Psi_{\mathrm{VBS}}(0)\rangle \sim \frac{1}{r^{2\dim\Psi_{\mathrm{VBS}}}} = \frac{1}{r^{\tilde{g}/2}}.$$

The phase transition between z-FM and VBS phase is tuned by λ, while at the critical point $\lambda = 0$ there exists an emergent O(2) symmetry corresponding to the $\tilde{\theta}$ part.

APPENDIX B: DETAILS OF RENORMALIZATION-GROUP CALCULATIONS FOR THE LONG-RANGE SINE-GORDON MODEL

In this work, we consider the long-range interaction Hamiltonian,

$$H_{\mathrm{LRP}} = \sum_i \left(-J_z S_i^z S_{i+1}^z + K_x S_i^x S_{i+2}^x + K_z S_i^z S_{i+2}^z\right) - \frac{J_z}{N(\alpha)}\sum_{i,j}\frac{S_i^z S_j^z}{|i-j|^\alpha}, \tag{B1}$$

where J is the interaction strength, and the parameter α tunes the power of long-range interactions. $N(\alpha)(=\frac{1}{N-1}\sum_{i\neq j}\frac{1}{|i-j|^\alpha})$ is the Kac factor to preserve the Hamiltonian extensively. To connect this model with the known short-range model (A1), we can separate the long-range term in the form

$$-\frac{J_z}{N(\alpha)}\sum_{i,j}\frac{S_i^z S_j^z}{|i-j|^\alpha} = -\frac{J_z}{N(\alpha)}\sum_{|i-j|=1} S_i^z S_j^z - \frac{J_z}{N(\alpha)}\sum_{|i-j|>1}\frac{S_i^z S_j^z}{|i-j|^\alpha} = -J_z'\sum_i S_i^z S_{i+1}^z - \frac{J_z}{N(\alpha)}\sum_{|i-j|>1}\frac{S_i^z S_j^z}{|i-j|^\alpha}.$$

Here the first term is just the conventional nearest-neighbor coupling. We consider the effective continuum theory for the long-range interactions,

$$\begin{aligned} H_{\mathrm{LR}} &= -\sum_{i,j}\frac{J_L}{|i-j|^\alpha}\sigma_i^z\sigma_j^z = -\sum_{i,j}\frac{J_L}{|i-j|^\alpha}\cos\phi_i\cos\phi_j \to -\int dxdx'\frac{J_L}{|x-x'|^\alpha}\cos\phi(x)\cos\phi(x') \\ &\to -\frac{1}{2}\int dxdr\frac{J_L}{|r|^\alpha}(\cos[\phi(x+r)-\phi(x)] + \cos[\phi(x+r)+\phi(x)]). \end{aligned} \tag{B2}$$

Expanding the first term for small r, we can obtain

$$\frac{1}{2}\int dxdr\frac{J_L}{|r|^\alpha}\cos[\phi(x+r)-\phi(x)] \approx \frac{1}{2}\int dxdr\frac{J_L}{|r|^\alpha}\left(1-\frac{1}{2}(r\nabla\phi)^2\right),$$

which only normalize the Luttinger parameters. In general, the long-range correlated interaction part of the action is given by

$$S_{\mathrm{LR}} = \frac{1}{2}\int d\tau\int dx\,dr\frac{1}{|r|^\alpha}(\lambda_+\cos[\phi(x+r,\tau)+\phi(x,\tau)] + \lambda_-\cos[\phi(x+r,\tau)-\phi(x,\tau)])$$

with the bare interaction strength $\lambda_+ < 0$ and $\lambda_- < 0$.

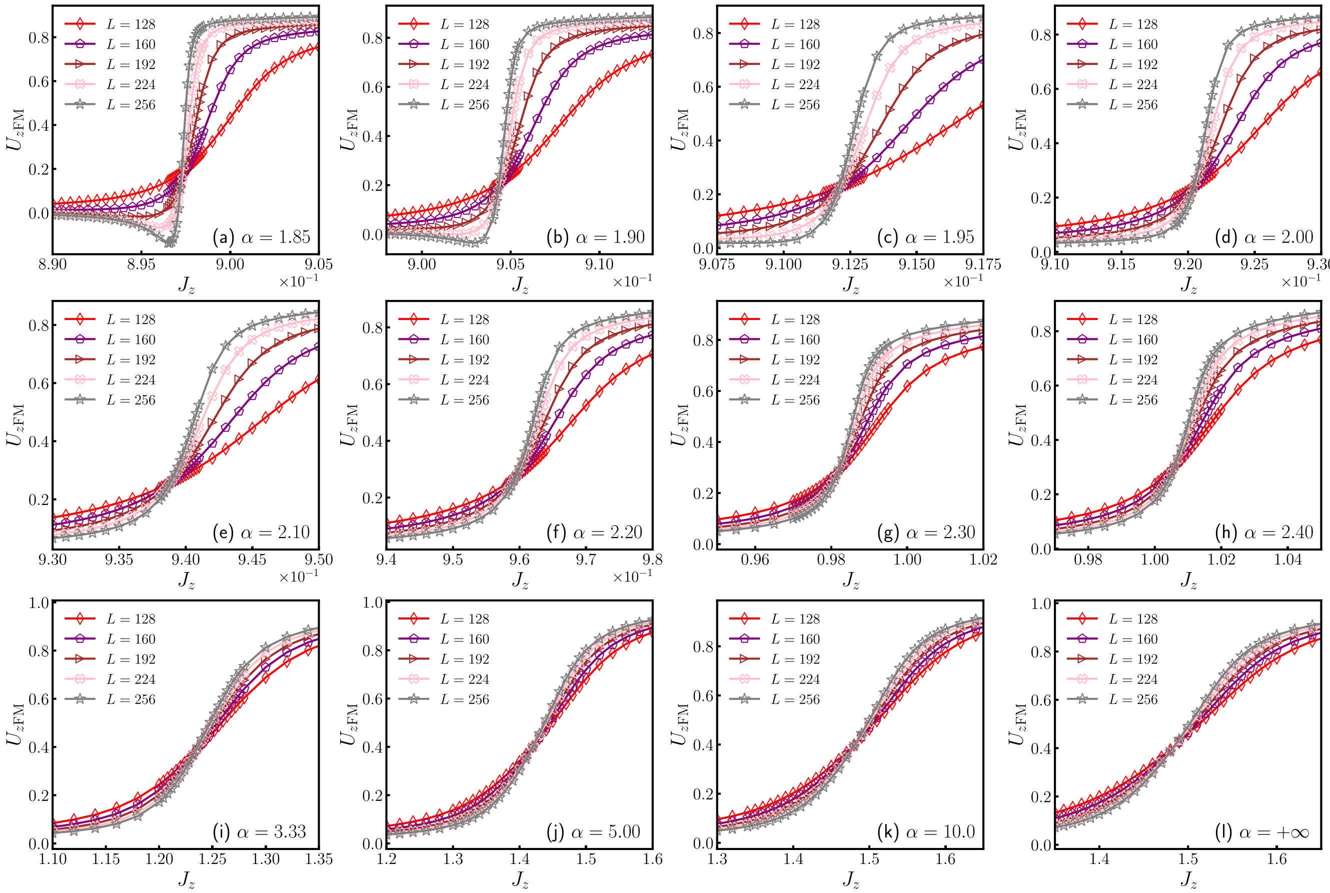

FIG. 6. The Binder ratio of the zFM order as a function of J_z for (a) $\alpha = 1.85$, (b) $\alpha = 1.90$, (c) $\alpha = 1.95$, (d) $\alpha = 2.00$, (e) $\alpha = 2.10$, (f) $\alpha = 2.20$, (g) $\alpha = 2.30$, (h) $\alpha = 2.40$, (i) $\alpha = 3.33$, (j) $\alpha = 5.00$, (k) $\alpha = 10.0$, and (l) $\alpha = +\infty$.

For the effective bosonization theory, we follow the conventional tree-level RG analysis of the sine-Gordon model [134]. Separating the field into slow and fast modes ($\phi = \phi_< + \phi_>$ and $\phi = \theta_< + \theta_>$) and integrating over the fast mode ($\phi_>, \theta_>$), the partition function can be expanded in the form

$$Z = \int D\phi D\theta\, e^{-S_0 - S_1} = \int D\phi_< D\theta_< \int D\phi_> D\theta_>\, e^{-S_{0,<} - S_{0,>} - S_1} = \int D\phi_< D\theta_<\, e^{-S_{0,<}} \sum_{n=0}^{\infty} \frac{1}{n!} \langle (-S_1)^n \rangle_>,$$

where the integral of the fast mode gives the average,

$$\langle \cdots \rangle_> \equiv \int D\phi_> D\theta_>\, e^{-S_{0,>}} (\cdots).$$

The effective action under the renormalization is

$$S_{\mathrm{eff}} = S_{0,<} + \langle S_1 \rangle_> - \tfrac{1}{2} \langle S_1^2 \rangle_{>,c}. \tag{B3}$$

The tree-level scalings of the operators can be obtained from the first-order term $\langle S_1 \rangle_>$. We consider the tree-level scaling for the long-range correlated terms,

$$\begin{aligned} S_\sigma &= \frac{1}{2} \lambda_\sigma \int d\tau \int dx dr \frac{1}{|r|^\alpha} \cos[\phi(x + r, \tau) + \sigma \phi(x, \tau)] \equiv \frac{1}{2} \lambda_\sigma \int d\tau \int dx dr \frac{1}{|r|^\alpha} \cos\left[\Delta_r^\sigma \phi\right] \\ &= \frac{1}{2} \lambda_\sigma \int d\tau \int dx dr \frac{1}{|r|^\alpha} \cos\left[\Delta_r^\sigma \phi_< + \Delta_r^\sigma \phi_>\right]. \end{aligned}$$

Integrating out the fast mode, the lowest-order correction is

$$\langle S_\sigma \rangle_> = \frac{1}{2} \lambda_\sigma \int d\tau \int dx dr \frac{1}{|r|^\alpha} \cos\left[\Delta_r^\sigma \phi_<\right] \left\langle \cos\left[\Delta_r^\sigma \phi_>\right] \right\rangle_>.$$

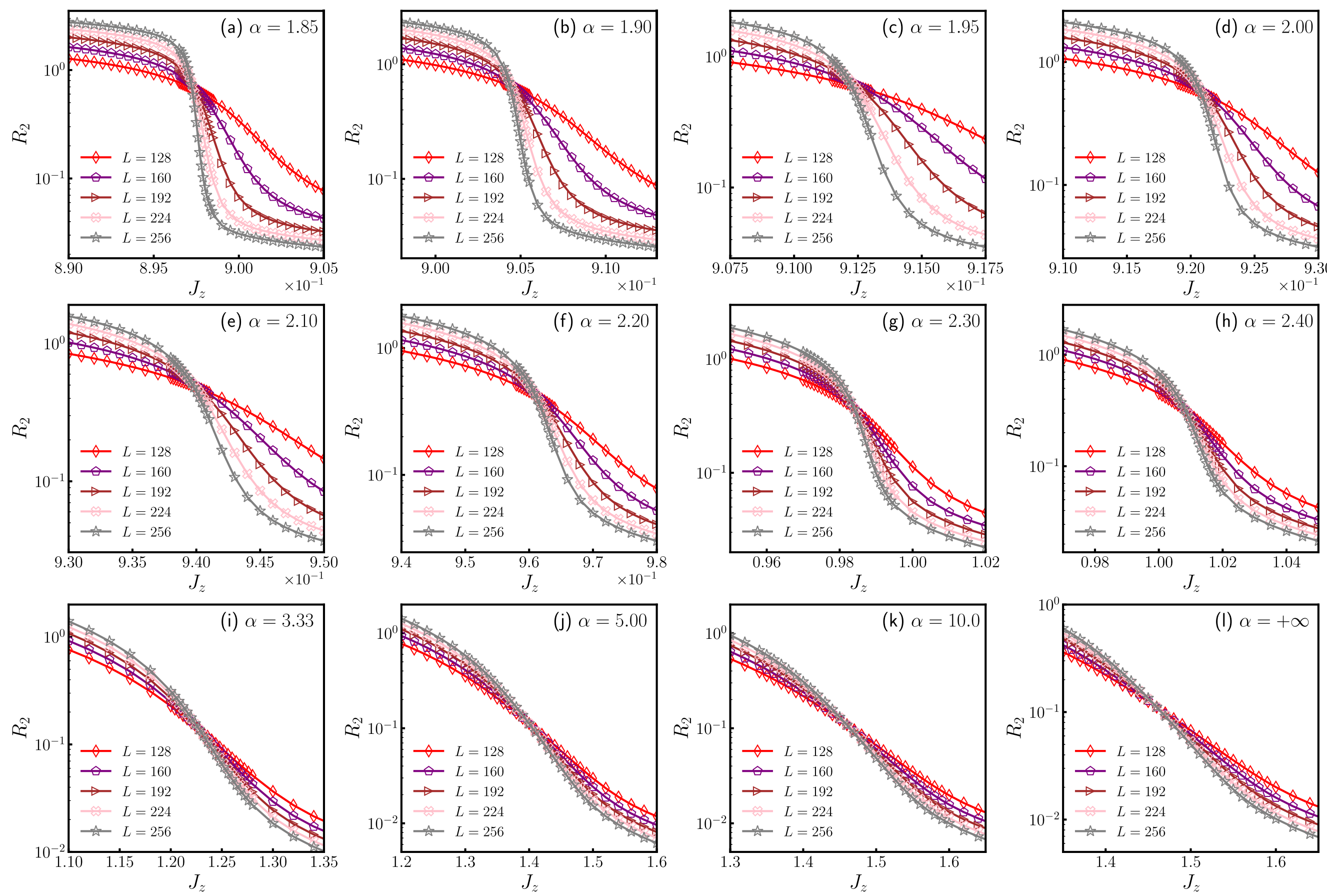

FIG. 7. The ratio of the squared order parameters R_2 as a function of J_z for (a) $\alpha = 1.85$, (b) $\alpha = 1.90$, (c) $\alpha = 1.95$, (d) $\alpha = 2.00$, (e) $\alpha = 2.10$, (f) $\alpha = 2.20$, (g) $\alpha = 2.30$, (h) $\alpha = 2.40$, (i) $\alpha = 3.33$, (j) $\alpha = 5.00$, (k) $\alpha = 10.0$, and (l) $\alpha = +\infty$.

Here, the renormalization gives the contribution

$$\begin{aligned}\left\langle \cos\left[\Delta_r^\sigma \phi_>\right]\right\rangle_> &= \exp\left(-\tfrac{1}{2}\left\langle\left[\Delta_r^\sigma \phi_>\right]^2\right\rangle_>\right) = \exp\left(-\tfrac{1}{2}\langle[\phi(x+r,\tau)+\sigma\phi(x,\tau)]^2\rangle_>\right)\\ &= \exp\left(-\tfrac{1}{2}\langle[\phi(r,0)+\sigma\phi(0)]^2\rangle_>\right),\end{aligned}$$

where the correlation function of $\phi(r)$ field can be calculated out directly,

$$\frac{1}{2}\langle[\phi(r,0)+\sigma\phi(0)]^2\rangle_> = \frac{1}{2}\int_> \frac{d\omega dq}{(2\pi)^2}(2+2\sigma\cos(|qr|))\frac{v}{g}\frac{\pi}{v^2q^2+\omega^2} = \frac{1}{2g}(1+\sigma\cos(|\Lambda r|))\frac{d\Lambda}{\Lambda}.$$

The lowest-order correction is

$$\langle S_\sigma\rangle_> = \frac{1}{2}\lambda_\sigma\int d\tau\int dxdr\frac{1}{|r|^\alpha}\cos\left[\Delta_r^\sigma\phi_<\right]\exp\left(-\frac{1}{2g}(1+\sigma\cos(|\Lambda r|))\frac{d\Lambda}{\Lambda}\right).$$

Up to tree level, the effective action under renormalization is $S_{\sigma,\mathrm{eff}} = S_{\sigma,<} + \langle S_\sigma\rangle_>$. Under the rescaling transformation,

$$\tau\to e^{dl}\tau,\quad x\to e^{dl}x,\quad r\to e^{dl}r,\quad \Lambda\to e^{-dl}\Lambda,$$

the effective action becomes

$$\begin{aligned}S_{\sigma,\mathrm{eff}} &\to \frac{1}{2}\lambda_\sigma e^{(3-\alpha)dl}\int d\tau\int dxdr\frac{1}{|r|^\alpha}\cos\left[\Delta_r^\sigma\phi\right]\left(1-\frac{1}{2g}dl-\frac{\sigma}{2g}\cos(|\Lambda r|)dl\right)\\ &= \frac{1}{2}\lambda_\sigma\int d\tau\int dxdr\frac{1}{|r|^\alpha}\cos\left[\Delta_r^\sigma\phi\right]\left(1+\left(3-\alpha-\frac{1}{2g}\right)dl-\frac{\sigma}{2g}\cos(|\Lambda r|)dl\right)\end{aligned}$$

and the RG functional equations for λ_σ are

$$\frac{d\lambda_\sigma(r)}{dl} = \left(3-\alpha-\frac{1+\sigma\cos(|\Lambda r|)}{2g}\right)\lambda_\sigma(r).$$

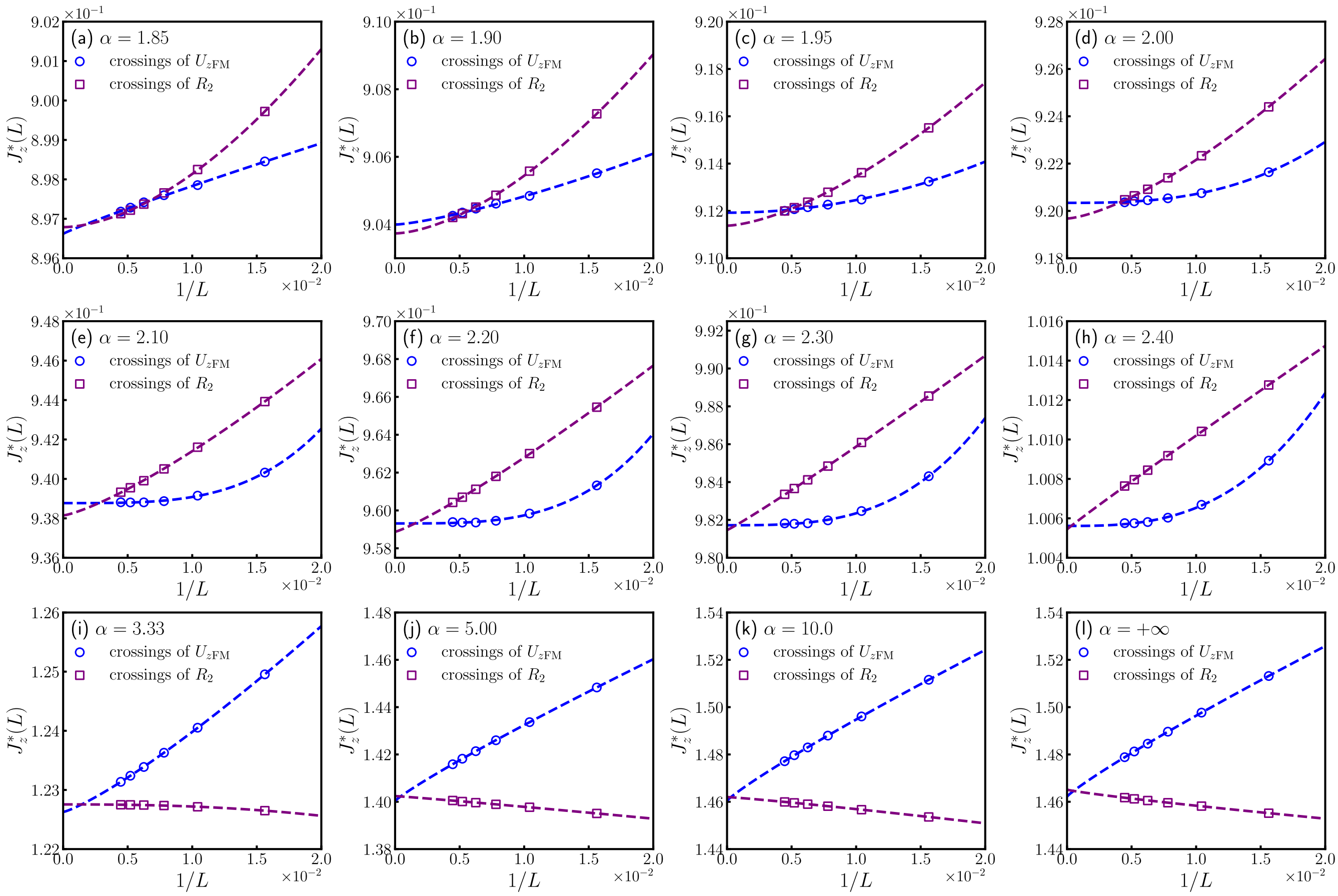

FIG. 8. The crossing locations $J_z^*(L)$ of $U_{z\mathrm{FM}}(L)$ [$R_2(L)$] and $U_{z\mathrm{FM}}(L+32)$ [$R_2(L+32)$] are shown vs $1/L$ for (a) $\alpha = 1.85$, (b) $\alpha = 1.90$, (c) $\alpha = 1.95$, (d) $\alpha = 2.00$, (e) $\alpha = 2.10$, (f) $\alpha = 2.20$, (g) $\alpha = 2.30$, (h) $\alpha = 2.40$, (i) $\alpha = 3.33$, (j) $\alpha = 5.00$, (k) $\alpha = 10.0$, and (l) $\alpha = +\infty$. The curves are least-squares fits according to $J_z^*(L) = J_z^c + aL^{-b}$. The critical points obtained, respectively, from $U_{z\mathrm{FM}}$ and R_2 are consistent with each other within numerical accuracy.

Here, the effective coupling has a nontrivial dependence on the momentum cutoff Λ. In the lattice formulation, the coordinates of the system are represented by $r = r_n = na$ ($n = 0, 1, \dots, N-1$), where a is the lattice constant, and the total lattice size is $L = Na$. The corresponding discrete set of momentum is $k = k_m = m\frac{\pi}{L} = m\frac{\pi}{Na}$ with $-\frac{N}{2}+1, \dots, \frac{N}{2}$. In the infrared (long-length) limit, the momentum will flow to the shortest momentum scale $\sim\pi/L$. For smaller r, the oscillation factor $\cos(|\Lambda r|)$ becomes nearly unity, and we can approximately obtain

$$r < r_c\!: \quad \frac{d\lambda_\sigma(r)}{dl} = \left(3 - \alpha - \frac{1+\sigma}{2g}\right)\lambda_\sigma(r).$$

For larger r, the scaling dimension of λ_- is bigger than λ_+. λ_- is more relevant than λ_+ in general. There exists a critical power α_c below which λ_σ becomes most relevant, dominating the physical behavior of the system.

Long-range interaction in the dual theory

We now transform to the effect of long-range interaction in the dual theory. From the representation of the order parameter in Eq. (A6), the long-range interaction in the continuous dual theory is given by

$$\begin{aligned} S_{\mathrm{LR}} &= \int d\tau \int dx dr \frac{\tilde{\lambda}}{|r|^\alpha} \sin[\tilde{\theta}(x+r,\tau)] \sin[\tilde{\theta}(x,\tau)] \\ &= \frac{1}{2} \int d\tau \int dx dr \frac{1}{|r|^\alpha} (\tilde{\lambda}_- \cos[\tilde{\theta}(x+r,\tau) - \tilde{\theta}(x,\tau)] - \tilde{\lambda}_+ \cos[\tilde{\theta}(x+r,\tau) + \tilde{\theta}(x,\tau)]). \end{aligned}$$

The renormalization of $\tilde{\lambda}_\pm$ takes the same form as $\lambda_\pm$, only taking the substitution $g \to 1/\tilde{g}$,

$$\frac{d\tilde{\lambda}_\sigma(r)}{dl} = \left(3 - \alpha - \tilde{g}\frac{1 + \sigma\cos(|\Lambda r|)}{2}\right)\tilde{\lambda}_\sigma(r).$$

As before, long-range $\tilde{\lambda}_-$ interaction will dominate the system when the power is smaller than some critical value, $\alpha < \alpha_c$. The scaling dimension of $\tilde{\lambda}_-$ is approximately given by

$$\dim[\tilde{\lambda}_-] = 3 - \alpha - \tilde{g}\frac{1-\delta}{2}$$

with some constant δ. Comparing the scaling dimension of the long-range $\tilde{\lambda}_-$ and short-range interaction λ at the tree level, we can obtain the critical power α_c,

$$3 - \alpha - \tilde{g}\frac{1-\delta}{2} = 2 - \tilde{g}, \quad \rightarrow \quad \alpha_c = 1 + \frac{\tilde{g}}{2}(\delta + 1).$$

The true critical power could lie between $1 + \frac{\tilde{g}}{2} < \alpha_c < 1 + \tilde{g}$.

APPENDIX C: ADDITIONAL DATA FOR zFM BINDER RATIO AND THE RATIO OF SQUARED ORDER PARAMETERS

In this Appendix, we provide additional results of the zFM Binder ratio $U_{z\mathrm{FM}}$ and the ratio of squared order parameters R_2 for other α values.

In Fig. 6, we first present $U_{z\mathrm{FM}}$ as a function of J_z for various system sizes at other representative α values. The distinct behaviors of $U_{z\mathrm{FM}}$ for $\alpha > \alpha_\mathrm{c}$ or $\alpha < \alpha_\mathrm{c}$ indicate a fundamental change of the transition nature as explained in the main text. An extrapolation of the crossing points of $U_{z\mathrm{FM}}$, according to the relation $J_z^*(L) = J_z^\mathrm{c} + aL^{-b}$, where $J_z^*(L)$ is the crossing point of $U_{z\mathrm{FM}}(L)$ and $U_{z\mathrm{FM}}(L + 32)$, is also performed to determine the precise boundary between the ordered phases (see Fig. 8). The obtained critical points are then used to complete the ground-state phase diagram displayed in the main text (see Fig. 1).

On the other hand, the ratio of squared order parameters R_2 versus J_z is also analyzed in Fig. 7 for other α values. It is clear that all the curves of different L intersect almost at a single point, which means that R_2 becomes universal at the critical point. The result can be supportive evidence for the $\mathrm{O}(2) \times \mathrm{O}(2)$ symmetry appearing along the whole transition line (the dashed line in Fig. 1). Furthermore, a similar extrapolation of the R_2 crossing points is also exhibited in Fig. 8, from which we can see that the extrapolated critical points are consistent with the ones extracted from $U_{z\mathrm{FM}}$ quite well.

[1] S. Sachdev, *Quantum Phases of Matter* (Cambridge University Press, Cambridge, England, 2023).

[2] S. Sachdev, *Quantum Phase Transitions*, 2nd ed. (Cambridge University Press, Cambridge, England, 2011).

[3] K. G. Wilson, The renormalization group and critical phenomena, Rev. Mod. Phys. **55**, 583 (1983).

[4] H. A. Kramers and G. H. Wannier, Statistics of the two-dimensional ferromagnet. Part I, Phys. Rev. **60**, 252 (1941).

[5] L. P. Kadanoff and H. Ceva, Determination of an operator algebra for the two-dimensional ising model, Phys. Rev. B **3**, 3918 (1971).

[6] C. Xu, Unconventional quantum critical points, Int. J. Mod. Phys. B **26**, 1230007 (2012).

[7] T. Senthil, L. Balents, S. Sachdev, A. Vishwanath, and M. P. A. Fisher, Quantum criticality beyond the landau-ginzburg-wilson paradigm, Phys. Rev. B **70**, 144407 (2004).

[8] T. Senthil, L. Balents, S. Sachdev, A. Vishwanath, and M. P. A. Fisher, Deconfined criticality critically defined, J. Phys. Soc. Jpn. **74**, 1 (2005).

[9] M. Levin and T. Senthil, Deconfined quantum criticality and néel order via dimer disorder, Phys. Rev. B **70**, 220403(R) (2004).

[10] T. Senthil and M. P. A. Fisher, Competing orders, nonlinear sigma models, and topological terms in quantum magnets, Phys. Rev. B **74**, 064405 (2006).

[11] B. Swingle and T. Senthil, Structure of entanglement at deconfined quantum critical points, Phys. Rev. B **86**, 155131 (2012).

[12] C. Wang, A. Nahum, M. A. Metlitski, C. Xu, and T. Senthil, Deconfined quantum critical points: Symmetries and dualities, Phys. Rev. X **7**, 031051 (2017).

[13] Z. Bi and T. Senthil, Adventure in topological phase transitions in 3 + 1-d: Non-abelian deconfined quantum criticalities and a possible duality, Phys. Rev. X **9**, 021034 (2019).

[14] Z. Bi, E. Lake, and T. Senthil, Landau ordering phase transitions beyond the landau paradigm, Phys. Rev. Res. **2**, 023031 (2020).

[15] S. Jiang and O. Motrunich, Ising ferromagnet to valence bond solid transition in a one-dimensional spin chain: Analogies to deconfined quantum critical points, Phys. Rev. B **99**, 075103 (2019).

[16] T. Senthil, Deconfined quantum critical points: A review, arXiv:2306.12638.

[17] Ö. M. Aksoy, C. Mudry, A. Furusaki, and A. Tiwari, Lieb-schultz-mattis anomalies and web of dualities induced by gauging in quantum spin chains, arXiv:2308.00743.

[18] M. A. Metlitski and R. Thorngren, Intrinsic and emergent anomalies at deconfined critical points, Phys. Rev. B **98**, 085140 (2018).

[19] N. Ma, G.-Y. Sun, Y.-Z. You, C. Xu, A. Vishwanath, A. W. Sandvik, and Z. Y. Meng, Dynamical signature of fractionalization at a deconfined quantum critical point, Phys. Rev. B **98**, 174421 (2018).

[20] Y. Q. Qin, Y.-Y. He, Y.-Z. You, Z.-Y. Lu, A. Sen, A. W. Sandvik, C. Xu, and Z. Y. Meng, Duality between the deconfined quantum-critical point and the bosonic topological transition, Phys. Rev. X **7**, 031052 (2017).

[21] A. W. Sandvik, Evidence for deconfined quantum criticality in a two-dimensional heisenberg model with four-spin interactions, Phys. Rev. Lett. **98**, 227202 (2007).

[22] A. Nahum, P. Serna, J. T. Chalker, M. Ortuño, and A. M. Somoza, Emergent so(5) symmetry at the néel to valence-bond-solid transition, Phys. Rev. Lett. **115**, 267203 (2015).

[23] N. Ma, Y.-Z. You, and Z. Y. Meng, Role of noether's theorem at the deconfined quantum critical point, Phys. Rev. Lett. **122**, 175701 (2019).

[24] R. Ma and C. Wang, Theory of deconfined pseudocriticality, Phys. Rev. B **102**, 020407(R) (2020).

[25] A. Nahum, Note on wess-zumino-witten models and quasiuniversality in $2+1$ dimensions, Phys. Rev. B **102**, 201116(R) (2020).

[26] D.-C. Lu, Nonlinear sigma model description of deconfined quantum criticality in arbitrary dimensions, arXiv:2209.00670.

[27] W. Ji, N. Tantivasadakarn, and C. Xu, Boundary states of three dimensional topological order and the deconfined quantum critical point, SciPost Phys. **15**, 231 (2023).

[28] S. Prembabu, R. Thorngren, and R. Verresen, Boundary deconfined quantum criticality at transitions between symmetry-protected topological chains, arXiv:2208.12258.

[29] C. Zhang and M. Levin, Exactly solvable model for a deconfined quantum critical point in 1d, Phys. Rev. Lett. **130**, 026801 (2023).

[30] V. Shyta, J. van den Brink, and F. S. Nogueira, Frozen deconfined quantum criticality, Phys. Rev. Lett. **129**, 227203 (2022).

[31] D. G. Joshi, C. Li, G. Tarnopolsky, A. Georges, and S. Sachdev, Deconfined critical point in a doped random quantum heisenberg magnet, Phys. Rev. X **10**, 021033 (2020).

[32] J. Y. Lee, Y.-Z. You, S. Sachdev, and A. Vishwanath, Signatures of a deconfined phase transition on the shastry-sutherland lattice: Applications to quantum critical $\mathrm{srcu_2(bo_3)_2}$, Phys. Rev. X **9**, 041037 (2019).

[33] Y.-Z. You, Y.-C. He, C. Xu, and A. Vishwanath, Symmetric fermion mass generation as deconfined quantum criticality, Phys. Rev. X **8**, 011026 (2018).

[34] C.-M. Jian, A. Thomson, A. Rasmussen, Z. Bi, and C. Xu, Deconfined quantum critical point on the triangular lattice, Phys. Rev. B **97**, 195115 (2018).

[35] C.-M. Jian, A. Rasmussen, Y.-Z. You, and C. Xu, Emergent symmetry and tricritical points near the deconfined quantum critical point, arXiv:1708.03050.

[36] L. Zou, Y.-C. He, and C. Wang, Stiefel liquids: Possible non-lagrangian quantum criticality from intertwined orders, Phys. Rev. X **11**, 031043 (2021).

[37] X.-Y. Song, C. Wang, A. Vishwanath, and Y.-C. He, Unifying description of competing orders in two-dimensional quantum magnets, Nat. Commun. **10**, 4254 (2019).

[38] X.-Y. Song, Y.-C. He, A. Vishwanath, and C. Wang, From spinon band topology to the symmetry quantum numbers of monopoles in dirac spin liquids, Phys. Rev. X **10**, 011033 (2020).

[39] L. Janssen and Y.-C. He, Critical behavior of the qed_3-gross-neveu model: Duality and deconfined criticality, Phys. Rev. B **96**, 205113 (2017).

[40] A. W. Sandvik, Continuous quantum phase transition between an antiferromagnet and a valence-bond solid in two dimensions: Evidence for logarithmic corrections to scaling, Phys. Rev. Lett. **104**, 177201 (2010).

[41] R. K. Kaul and A. W. Sandvik, Lattice model for the SU(n) néel to valence-bond solid quantum phase transition at large n, Phys. Rev. Lett. **108**, 137201 (2012).

[42] A. W. Sandvik and B. Zhao, Consistent scaling exponents at the deconfined quantum-critical point*, Chin. Phys. Lett. **37**, 057502 (2020).

[43] H. Shao, W. Guo, and Anders W Sandvik, Quantum criticality with two length scales, Science **352**, 213 (2016).

[44] M. S. Block, R. G. Melko, and R. K. Kaul, Fate of $\mathbb{C}\mathbb{P}^{N-1}$ fixed points with q monopoles, Phys. Rev. Lett. **111**, 137202 (2013).

[45] R. K. Kaul and R. G. Melko, Large-n estimates of universal amplitudes of the $\mathbb{C}\mathbb{P}^{N-1}$ theory and comparison with an $s=\frac{1}{2}$ square-lattice model with competing four-spin interactions, Phys. Rev. B **78**, 014417 (2008).

[46] Y. Nakayama and T. Ohtsuki, Necessary condition for emergent symmetry from the conformal bootstrap, Phys. Rev. Lett. **117**, 131601 (2016).

[47] Y.-C. He, J. Rong, and N. Su, Non-Wilson-Fisher kinks of $O(N)$ numerical bootstrap: from the deconfined phase transition to a putative new family of CFTs, SciPost Phys. **10**, 115 (2021).

[48] Y.-R. Shu, S.-K. Jian, A. W. Sandvik, and S. Yin, Equilibration of topological defects at the deconfined quantum critical point, arXiv:2305.04771.

[49] Z.-X. Li, S.-K. Jian, and H. Yao, Deconfined quantum criticality and emergent so(5) symmetry in fermionic systems, arXiv:1904.10975.

[50] D.-X. Liu, Z. Xiong, Y. Xu, and X.-F. Zhang, Does deconfined quantum phase transition have to keep lorentz symmetry? two velocities of spinon and string, arXiv:2301.12864.

[51] X.-F. Zhang, Y.-C. He, S. Eggert, R. Moessner, and F. Pollmann, Continuous easy-plane deconfined phase transition on the kagome lattice, Phys. Rev. Lett. **120**, 115702 (2018).

[52] B.-B. Chen, X. Zhang, Y. Wang, K. Sun, and Z. Y. Meng, Phases of (2+1)d so(5) non-linear sigma model with a topological term on a sphere: multicritical point and disorder phase, arXiv:2307.05307.

[53] M. Song, J. Zhao, L. Janssen, M. M. Scherer, and Z. Y. Meng, Deconfined quantum criticality lost, arXiv:2307.02547.

[54] Z. H. Liu, W. Jiang, B.-B. Chen, J. Rong, M. Cheng, K. Sun, Z. Y. Meng, and F. F. Assaad, Fermion disorder operator at gross-neveu and deconfined quantum criticalities, Phys. Rev. Lett. **130**, 266501 (2023).

[55] Y. D. Liao, X. Y. Xu, Z. Y. Meng, and Y. Qi, Dirac fermions with plaquette interactions. I. su(2) phase diagram with gross-neveu and deconfined quantum criticalities, Phys. Rev. B **106**, 075111 (2022).

[56] J. Zhao, Y.-C. Wang, Z. Yan, M. Cheng, and Z. Y. Meng, Scaling of entanglement entropy at deconfined quantum criticality, Phys. Rev. Lett. **128**, 010601 (2022).

[57] Y.-C. Wang, N. Ma, M. Cheng, and Z. Y. Meng, Scaling of the disorder operator at deconfined quantum criticality, SciPost Phys. **13**, 123 (2022).

[58] Y. D. Liao, G. Pan, W. Jiang, Y. Qi, and Z. Y. Meng, The teaching from entanglement: 2d su(2) antiferromagnet to valence bond solid deconfined quantum critical points are not conformal, arXiv:2302.11742.

[59] W.-Y. Liu, S.-S. Gong, W.-Q. Chen, and Z.-C. Gu, Emergent symmetry in frustrated magnets: From deconfined

quantum critical point to gapless quantum spin liquid, arXiv:2212.00707.

[60] Y.-Z. You and J. Wang, Deconfined quantum criticality among grant unified theories, in *A Festschrift in Honor of the C N Yang Centenary* (World Scientific, Singapore, 2022), pp. 367–383.

[61] N. Xi and R. Yu, Dynamical signatures of the one-dimensional deconfined quantum critical point, Chin. Phys. B **31**, 057501 (2022).

[62] Y.-R. Shu and S. Yin, Dual dynamic scaling in deconfined quantum criticality, Phys. Rev. B **105**, 104420 (2022).

[63] W.-Y. Liu, J. Hasik, S.-S. Gong, D. Poilblanc, W.-Q. Chen, and Z.-C. Gu, Emergence of gapless quantum spin liquid from deconfined quantum critical point, Phys. Rev. X **12**, 031039 (2022).

[64] Z. H. Liu, M. Vojta, F. F. Assaad, and L. Janssen, Metallic and deconfined quantum criticality in dirac systems, Phys. Rev. Lett. **128**, 087201 (2022).

[65] Y.-R. Shu, S.-K. Jian, and S. Yin, Nonequilibrium dynamics of deconfined quantum critical point in imaginary time, Phys. Rev. Lett. **128**, 020601 (2022).

[66] R.-Z. Huang and S. Yin, Kibble-zurek mechanism for a one-dimensional incarnation of a deconfined quantum critical point, Phys. Rev. Res. **2**, 023175 (2020).

[67] T.-S. Zeng, D. N. Sheng, and W. Zhu, Continuous phase transition between bosonic integer quantum hall liquid and a trivial insulator: Evidence for deconfined quantum criticality, Phys. Rev. B **101**, 035138 (2020).

[68] G. Sun, B.-B. Wei, and S.-P. Kou, Fidelity as a probe for a deconfined quantum critical point, Phys. Rev. B **100**, 064427 (2019).

[69] B. Roberts, S. Jiang, and O. I. Motrunich, Deconfined quantum critical point in one dimension, Phys. Rev. B **99**, 165143 (2019).

[70] A. Nahum, J. T. Chalker, P. Serna, M. Ortuño, and A. M. Somoza, Deconfined quantum criticality, scaling violations, and classical loop models, Phys. Rev. X **5**, 041048 (2015).

[71] Z. Zhou, L. Hu, W. Zhu, and Y.-C. He, The SO(5) deconfined phase transition under the fuzzy sphere microscope: Approximate conformal symmetry, pseudo-criticality, and operator spectrum, arXiv:2306.16435.

[72] Y. Liu, Z. Wang, T. Sato, M. Hohenadler, C. Wang, W. Guo, and F. F. Assaad, Superconductivity from the condensation of topological defects in a quantum spin-hall insulator, Nat. Commun. **10**, 2658 (2019).

[73] J. D'Emidio, Lee-yang zeros at $o(3)$ and deconfined quantum critical points, arXiv:2308.00575.

[74] J. D'Emidio and R. K. Kaul, New easy-plane $\mathbb{CP}^{N-1}$ fixed points, Phys. Rev. Lett. **118**, 187202 (2017).

[75] K. Chen, Y. Huang, Y. Deng, A. B. Kuklov, N. V. Prokof'ev, and B. V. Svistunov, Deconfined criticality flow in the heisenberg model with ring-exchange interactions, Phys. Rev. Lett. **110**, 185701 (2013).

[76] J. Guo, G. Sun, B. Zhao, L. Wang, W. Hong, V. A. Sidorov, N. Ma, Q. Wu, S. Li, Z. Y. Meng, A. W. Sandvik, and L. Sun, Quantum phases of $\mathrm{srcu}_2(\mathrm{bo}_3)_2$ from high-pressure thermodynamics, Phys. Rev. Lett. **124**, 206602 (2020).

[77] Y. Cui, L. Liu, H. Lin, K.-H. Wu, W. Hong, X. Liu, C. Li, Z. Hu, N. Xi, S. Li *et al.*, Proximate deconfined quantum critical point in srcu2 (bo3) 2, Science **380**, 1179 (2023).

[78] T. Song, Y. Jia, G. Yu, Y. Tang, P. Wang, R. Singha, X. Gui, A. J. Uzan, M. Onyszczak, K. Watanabe, T. Taniguchi, R. J. Cava, L. M. Schoop, N. P. Ong, and S. Wu, Unconventional superconducting quantum criticality in monolayer wte2, arXiv:2303.06540.

[79] M. Saffman, T. G. Walker, and K. Mølmer, Quantum information with Rydberg atoms, Rev. Mod. Phys. **82**, 2313 (2010).

[80] X.-L. Deng, D. Porras, and J. I. Cirac, Effective spin quantum phases in systems of trapped ions, Phys. Rev. A **72**, 063407 (2005).

[81] T. Lahaye, C. Menotti, L. Santos, M. Lewenstein, and T. Pfau, The physics of dipolar bosonic quantum gases, Rep. Prog. Phys. **72**, 126401 (2009).

[82] H. Ritsch, P. Domokos, F. Brennecke, and T. Esslinger, Cold atoms in cavity-generated dynamical optical potentials, Rev. Mod. Phys. **85**, 553 (2013).

[83] L. D. Carr, D. DeMille, R. V. Krems, and J. Ye, Cold and ultracold molecules: science, technology and applications, New J. Phys. **11**, 055049 (2009).

[84] R. Blatt and C. F. Roos, Quantum simulations with trapped ions, Nat. Phys. **8**, 277 (2012).

[85] J. W. Britton, B. C. Sawyer, A. C. Keith, C.-C. J. Wang, J. K. Freericks, H. Uys, M. J. Biercuk, and J. J. Bollinger, Engineered two-dimensional ising interactions in a trapped-ion quantum simulator with hundreds of spins, Nature (London) **484**, 489 (2012).

[86] R. Islam, C. Senko, W. C. Campbell, S. Korenblit, J. Smith, A. Lee, E. E. Edwards, C.-C. J. Wang, J. K. Freericks, and C. Monroe, Emergence and frustration of magnetism with variable-range interactions in a quantum simulator, Science **340**, 583 (2013).

[87] P. Richerme, Z.-X. Gong, A. Lee, C. Senko, J. Smith, M. Foss-Feig, S. Michalakis, A. V. Gorshkov, and C. Monroe, Non-local propagation of correlations in quantum systems with long-range interactions, Nature (London) **511**, 198 (2014).

[88] P. Jurcevic, B. P. Lanyon, P. Hauke, C. Hempel, P. Zoller, R. Blatt, and C. F. Roos, Quasiparticle engineering and entanglement propagation in a quantum many-body system, Nature (London) **511**, 202 (2014).

[89] X.-J. Yu, S. Yang, J.-B. Xu, and L. Xu, Fidelity susceptibility as a diagnostic of the commensurate-incommensurate transition: A revisit of the programmable rydberg chain, Phys. Rev. B **106**, 165124 (2022).

[90] N. Defenu, T. Enss, M. Kastner, and G. Morigi, Dynamical critical scaling of long-range interacting quantum magnets, Phys. Rev. Lett. **121**, 240403 (2018).

[91] N. Defenu, T. Donner, T. Macrì, G. Pagano, S. Ruffo, and A. Trombettoni, Long-range interacting quantum systems, arXiv:2109.01063.

[92] N. Defenu, A. Lerose, and S. Pappalardi, Out-of-equilibrium dynamics of quantum many-body systems with long-range interactions, arXiv:2307.04802.

[93] M. Syed, T. Enss, and N. Defenu, Dynamical quantum phase transition in a bosonic system with long-range interactions, Phys. Rev. B **103**, 064306 (2021).

[94] N. Defenu, A. Trombettoni, and S. Ruffo, Anisotropic long-range spin systems, Phys. Rev. B **94**, 224411 (2016).

[95] Z.-X. Gong, M. F. Maghrebi, A. Hu, M. L. Wall, M. Foss-Feig, and A. V. Gorshkov, Topological phases with long-range interactions, Phys. Rev. B **93**, 041102(R) (2016).
[96] Z.-X. Gong, M. F. Maghrebi, A. Hu, M. Foss-Feig, P. Richerme, C. Monroe, and A. V. Gorshkov, Kaleidoscope of quantum phases in a long-range interacting spin-1 chain, Phys. Rev. B **93**, 205115 (2016).
[97] X. Shen, Long range syk model and boundary syk model, arXiv:2308.12598.
[98] M. E. Fisher, S.-K. Ma, and B. G. Nickel, Critical exponents for long-range interactions, Phys. Rev. Lett. **29**, 917 (1972).
[99] N. Defenu, A. Trombettoni, and S. Ruffo, Criticality and phase diagram of quantum long-range o(n) models, Phys. Rev. B **96**, 104432 (2017).
[100] N. Defenu, A. Codello, S. Ruffo, and A. Trombettoni, Criticality of spin systems with weak long-range interactions, J. Phys. A **53**, 143001 (2020).
[101] G. Giachetti, N. Defenu, S. Ruffo, and A. Trombettoni, Berezinskii-kosterlitz-thouless phase transitions with long-range couplings, Phys. Rev. Lett. **127**, 156801 (2021).
[102] G. Giachetti, A. Trombettoni, S. Ruffo, and N. Defenu, Berezinskii-kosterlitz-thouless transitions in classical and quantum long-range systems, Phys. Rev. B **106**, 014106 (2022).
[103] A. Codello, N. Defenu, and G. D'Odorico, Critical exponents of $o(n)$ models in fractional dimensions, Phys. Rev. D **91**, 105003 (2015).
[104] M. Song, J. Zhao, C. Zhou, and Z. Y. Meng, Dynamical properties of quantum many-body systems with long range interactions, Phys. Rev. Res. **5**, 033046 (2023).
[105] M. Song, J. Zhao, Y. Qi, J. Rong, and Z. Y. Meng, Quantum criticality and entanglement for 2d long-range Heisenberg Bilayer, arXiv:2306.05465.
[106] J. Zhao, M. Song, Y. Qi, J. Rong, and Z. Y. Meng, Finite-temperature critical behaviors in 2d long-range quantum Heisenberg model, npj Quantum Mater. **8**, 59 (2023).
[107] N. Defenu, A. Trombettoni, and A. Codello, Fixed-point structure and effective fractional dimensionality for o(n) models with long-range interactions, Phys. Rev. E **92**, 052113 (2015).
[108] M. F. Maghrebi, Z.-X. Gong, M. Foss-Feig, and A. V. Gorshkov, Causality and quantum criticality in long-range lattice models, Phys. Rev. B **93**, 125128 (2016).
[109] M. F. Maghrebi, Z.-X. Gong, and A. V. Gorshkov, Continuous symmetry breaking in 1d long-range interacting quantum systems, Phys. Rev. Lett. **119**, 023001 (2017).
[110] S. Yang, D.-X. Yao, and A. W. Sandvik, Deconfined quantum criticality in spin-1/2 chains with long-range interactions, arXiv:2001.02821.
[111] A. W. Sandvik, Ground states of a frustrated quantum spin chain with long-range interactions, Phys. Rev. Lett. **104**, 137204 (2010).
[112] X.-J. Yu, C. Ding, and L. Xu, Quantum criticality of a $\mathbb{Z}_3$-symmetric spin chain with long-range interactions, Phys. Rev. E **107**, 054122 (2023).
[113] D. Vu, K. Huang, X. Li, and S. Das Sarma, Fermionic many-body localization for random and quasiperiodic systems in the presence of short- and long-range interactions, Phys. Rev. Lett. **128**, 146601 (2022).
[114] J. N. Leaw, H.-K. Tang, M. Trushin, F. F. Assaad, and S. Adam, Universal fermi-surface anisotropy renormalization for interacting Dirac fermions with long-range interactions, Proc. Natl. Acad. Sci. USA **116**, 26431 (2019).
[115] A. Ghazaryan and T. Chakraborty, Long-range coulomb interaction and majorana fermions, Phys. Rev. B **92**, 115138 (2015).
[116] D. Vodola, L. Lepori, E. Ercolessi, A. V. Gorshkov, and G. Pupillo, Kitaev chains with long-range pairing, Phys. Rev. Lett. **113**, 156402 (2014).
[117] C. Mudry, A. Furusaki, T. Morimoto, and T. Hikihara, Quantum phase transitions beyond Landau-Ginzburg theory in one-dimensional space revisited, Phys. Rev. B **99**, 205153 (2019).
[118] R.-Z. Huang, D.-C. Lu, Y.-Z. You, Z. Y. Meng, and T. Xiang, Emergent symmetry and conserved current at a one-dimensional incarnation of deconfined quantum critical point, Phys. Rev. B **100**, 125137 (2019).
[119] S. R. White, Density matrix formulation for quantum renormalization groups, Phys. Rev. Lett. **69**, 2863 (1992).
[120] U. Schollwöck, The density-matrix renormalization group, Rev. Mod. Phys. **77**, 259 (2005).
[121] U. Schollwöck, The density-matrix renormalization group in the age of matrix product states, Ann. Phys. **326**, 96 (2011).
[122] F. Verstraete, D. Porras, and J. I. Cirac, Density matrix renormalization group and periodic boundary conditions: A quantum information perspective, Phys. Rev. Lett. **93**, 227205 (2004).
[123] G. Nigel, *Lectures on Phase Transitions and the Renormalization Group*, 1st ed. (CRC Press, Boca Raton, FL, 1992).
[124] Q. Luo, J. Zhao, and X. Wang, Intrinsic jump character of first-order quantum phase transitions, Phys. Rev. B **100**, 121111(R) (2019).
[125] Q. Luo, S. Hu, J. Li, J. Zhao, H.-Y. Kee, and X. Wang, Spontaneous dimerization, spin-nematic order, and deconfined quantum critical point in a spin-1 Kitaev chain with tunable single-ion anisotropy, Phys. Rev. B **107**, 245131 (2023).
[126] K. Binder, Finite size scaling analysis of Ising model block distribution functions, Z. Phys. B **43**, 119 (1981).
[127] K. Vollmayr, J. D. Reger, M. Scheucher, and K. Binder, Finite size effects at thermally-driven first order phase transitions: A phenomenological theory of the order parameter distribution, Z. Phys. B **91**, 113 (1993).
[128] A. W. Sandvik, Computational studies of quantum spin systems, AIP Conf. Proc. No. **1297** (AIP, New York, 2010), pp. 135–338.
[129] Y.-C. Wang, Y. Qi, S. Chen, and Z. Y. Meng, Caution on emergent continuous symmetry: A Monte Carlo investigation of the transverse-field frustrated Ising model on the triangular and Honeycomb lattices, Phys. Rev. B **96**, 115160 (2017).
[130] A. Kuklov, N. V. Prokof'Ev, B. V. Svistunov, and M. Troyer, Deconfined criticality, runaway flow in the two-component scalar electrodynamics and weak first-order superfluid-solid transitions, Ann. Phys. **321**, 1602 (2006).
[131] G. J. Sreejith, S. Powell, and A. Nahum, Emergent so(5) symmetry at the columnar ordering transition in the classical cubic dimer model, Phys. Rev. Lett. **122**, 080601 (2019).
[132] P. Serna and A. Nahum, Emergence and spontaneous breaking of approximate O(4) symmetry at a weakly first-order deconfined phase transition, Phys. Rev. B **99**, 195110 (2019).

[133] T. Sato, M. Hohenadler, and F. F. Assaad, Dirac fermions with competing orders: Non-Landau transition with emergent symmetry, Phys. Rev. Lett. **119**, 197203 (2017).
[134] T. Giamarchi, *Quantum Physics in One Dimension* (Clarendon Press, Oxford, England, 2003), Vol. 121.
[135] C.-N. Yang and C.-P. Yang, One-dimensional chain of anisotropic spin-spin interactions. I. Proof of Bethe's hypothesis for ground state in a finite system, Phys. Rev. **150**, 321 (1966).
[136] C.-N. Yang and C.-P. Yang, One-dimensional chain of anisotropic spin-spin interactions. II. Properties of the ground-state energy per lattice site for an infinite system, Phys. Rev. **150**, 327 (1966).
[137] C.-N. Yang and C.-P. Yang, One-dimensional chain of anisotropic spin-spin interactions. III. Applications, Phys. Rev. **151**, 258 (1966).
[138] D.-C. Lu, C. Xu, and Y.-Z. You, Self-duality protected multicriticality in deconfined quantum phase transitions, Phys. Rev. B **104**, 205142 (2021).
[139] B. Zhao, P. Weinberg, and A. W. Sandvik, Symmetry-enhanced discontinuous phase transition in a two-dimensional quantum magnet, Nat. Phys. **15**, 678 (2019).
[140] G. Sun, N. Ma, B. Zhao, A. W. Sandvik, and Z. Y. Meng, Emergent o(4) symmetry at the phase transition from plaquette-singlet to antiferromagnetic order in quasi-two-dimensional quantum magnets, Chin. Phys. B **30**, 067505 (2021).
[141] J. Wildeboer, N. Desai, J. D'Emidio, and R. K. Kaul, First-order néel to columnar valence bond solid transition in a model square-lattice $s = 1$ antiferromagnet, Phys. Rev. B **101**, 045111 (2020).
[142] J. Yu, R. Roiban, S.-K. Jian, and C.-X. Liu, Finite-scale emergence of $2 + 1$D supersymmetry at first-order quantum phase transition, Phys. Rev. B **100**, 075153 (2019).
[143] J. Y. Lee, J. Ramette, M. A. Metlitski, V. Vuletic, W. W. Ho, and S. Choi, Landau-forbidden quantum criticality in Rydberg quantum simulators, Phys. Rev. Lett. **131**, 083601 (2023).
[144] C.-M. Chang, Y.-H. Lin, S.-H. Shao, Y. Wang, and X. Yin, Topological defect lines and renormalization group flows in two dimensions, J. High Energy Phys. 01 (2019) 026.
[145] R. Thorngren and Y. Wang, Fusion category symmetry II: Categoriosities at c= 1 and beyond, arXiv:2106.12577.
[146] M. Fishman, S. R. White, and E. M. Stoudenmire, The ITensor Software Library for Tensor Network Calculations, SciPost Phys. Codebases 4 (2022).